Thermally activated resonant tunnelling in GaAs/AlGaAs triple barrier heterostructures

2015 Semicond. Sci. Technol. 30 105035

(http://iopscience.iop.org/0268-1242/30/10/105035)

OPEN ACCESS
IOP Publishing
Semiconductor Science and Technology
Semicond. Sci. Technol. **30** (2015) 105035 (7pp)
doi:10.1088/0268-1242/30/10/105035

Thermally activated resonant tunnelling in GaAs/AlGaAs triple barrier heterostructures

C P Allford[1], R E Legg[1], R A O'Donnell[1], P Dawson[2], M Missous[3] and P D Buckle[1]

[1] School of Physics and Astronomy, Cardiff University, Queen's Buildings, The Parade, Cardiff, CF24 3AA, UK
[2] The School of Physics and Astronomy, Photon Science Institute, Alan Turing Building, The University of Manchester, Manchester, M13 9PL, UK
[3] School of Electrical and Electronic Engineering, Sackville Street Building, The University of Manchester, M13 9PL, UK

E-mail: allfordcp1@cardiff.ac.uk

Received 30 April 2015, revised 5 August 2015
Accepted for publication 13 August 2015
Published 21 September 2015

Abstract

We report the observation of a thermally activated resonant tunnelling feature in the current–voltage characteristics ($I(V)$) of triple barrier resonant tunnelling structures (TBRTS) due to the alignment of the $n = 1$ confined states of the two quantum wells within the active region. With great renewed interest in tunnelling structures for high frequency (THz) operation, the understanding of device transport and charge accumulation as a function of temperature is critical. With rising sample temperature, the tunnelling current of the observed low voltage resonant feature increases in magnitude showing a small negative differential resistance region which is discernible even at 293 K and is unique to multiple barrier devices. This behaviour is not observed in conventional double barrier resonant tunnelling structures where the transmission coefficient at the Fermi energy is predominantly controlled by an electric field, whereas in TBRTS it is strongly controlled by the 2D to 2D state alignment.

Keywords: resonant tunnelling, semiconductor heterostructures, triple barriers

(Some figures may appear in colour only in the online journal)

1. Introduction

Semiconductor multi-barrier tunnelling structures, where the quantum well (QW) confined states are strongly coupled, have attracted considerable interest over a number of years for both fundamental investigations of tunnelling processes and electronic and optoelectronic applications. Pessimism concerning high frequency operation has proved unfounded with estimates of THz gain in triple barrier resonant tunnelling structures (TBRTS) [1] and now a number of reports of measured THz operation in conventional double barrier structures [2–5]. Interest in TBRTS was originally generated by the possibility of creating multiple negative differential resistance (NDR) regions in the current–voltage $I(V)$ characteristics, where the peak currents are of similar magnitude. These devices could therefore be used for triple valued logic and memory applications [6–8]. In the case of more fundamental studies coupled QW systems have proved to be a very rich area for studying physical phenomena associated with quantum interference and coherent electron oscillations [9–11], and it has been proposed that such quantum oscillations in multi-barrier tunnelling structures can be utilized in devices which can be operated at terahertz frequencies [12, 13]. These devices overcome some of the problems suggested in reports on conventional double barrier resonant tunnelling devices (DBRTS), where access resistance was thought to limit the ultimate frequency of oscillation [14]. Different materials systems have been explored to minimize this access resistance, but with no reports of high frequency operation at that time [15].

The basic operational principle of a DBRTS is that the injection energy of carriers incident on the emitter barrier is altered by the application of an electric field. This is also true for injection into the states of the QW adjacent to the emitter in a TBRTS, however the relative alignment of quasi-confined states in the two QWs of the TBRTS has a strong effect on the transmission through the device.

The first report of resonant tunnelling in TBRTS was by Nakagawa *et al* [16]. It was demonstrated that the resonant features in the $I(V)$ characteristics of triple barrier devices may be stronger than those observed in the more widely studied (DBRTS) [17, 18] due to an effective suppression of the off resonant current. It was pointed out in this work that under certain conditions a TBRTS can be viewed as a conventional double barrier resonant tunnelling structure (DBRTS) with a modified emitter that acts as an energy filter for injected electrons. Similar concepts were explored in studies of charge build up treating the emitter or collector well as a wide barrier under specific bias conditions [19]. The QW state alignment in TBRTS can provide far more variation in transmission coefficient as a function of applied voltage than in a conventional DBRTS, and also leads to resonance effects in the $I(V)$ characteristics of both symmetric and asymmetric QW TBRTS whose magnitude increases with increasing temperature. A resonance similar to this in behaviour was shown in presented data by Nakagawa *et al* [20] but not considered or commented on in the paper text which focused on higher energy state resonances. Phonon assisted tunnelling in similar structures has also been reported by Ozaki *et al* [21]. In these structures it was demonstrated that electrons tunnelling into the first QW (emitter QW) can be thermally promoted to excited states ($n > 1$) within the emitter QW and can then tunnel to an energetically aligned excited state in the second QW (collector QW) of the TBRTS.

In this paper we present temperature dependent $I(V)$ measurements on TBRTS which demonstrate that a large thermally enhanced resonant tunnelling current can occur through the alignment of the $n = 1$ states in the emitter and collector QWs. We demonstrate that such a resonance is observable even when this critical alignment occurs well above that of the Fermi energy in the emitter, thus enabling an extremely low bias resonance to be achieved for a nominally symmetric structure.

2. Experimental details

The structures studied in this paper were grown by solid source molecular beam epitaxy on semi-insulating GaAs substrates. The symmetric barrier TBRTS with either symmetric or asymmetric QW's comprised of the following layers

(i) 1 μm n+ ($n = 7 \times 10^{18}$ cm^{-3}) GaAs buffer layer,
(ii) 100 Å doped ($n = 3 \times 10^{17}$ cm^{-3}) GaAs layer,
(iii) 100 Å undoped GaAs spacer layer,
(iv) 45 Å $Al_{0.33}Ga_{0.67}As$ barrier,
(v) Nominally 65 Å undoped GaAs QW,
(vi) 54 Å $Al_{0.33}Ga_{0.67}As$ barrier,
(vii) Undoped GaAs QW of nominal widths 45, 48, 51, 54, 57, 59, 62 Å for the asymmetric QW devices, and 65 Å for the symmetric QW device,
(viii) 45 Å $Al_{0.33}Ga_{0.67}As$ barrier,
(ix) 200 Å GaAs spacer layer,
(x) $n = 5 \times 10^{12}$ cm^{-2} Si δ-doped layer,
(xi) 0.4 μm n+ ($n = 7 \times 10^{18}$ cm^{-3}) contact layer.

The layer structure is shown schematically in figure 1(a). Device structures were fabricated by conventional photolithography into 50 × 50 μm mesas, (shown in figure 1(b)). Top and bottom ohmic contacts were formed by evaporating AuGe/Ni/Au and alloying by rapid thermal annealing at 395 °C. The devices were mounted in 20-way ceramic packages and mounted on the cold finger of a closed cycle helium pulse tube cryostat. Current–voltage ($I(V)$) characteristics between ±0.6 V for both forward and reverse going directions were measured using a four wire technique at temperatures from 3 K to 293 K at 2 K intervals. Conduction band potential profiles of both symmetric and asymmetric structures calculated from a self consistent Schrödinger–Poisson model at zero bias are shown in figures 1(c) and (e) respectively, with the calculated electron probability density for the lowest significant confined states showing the alignment of the QW states for the symmetric structure and misalignment of the QW states for the asymmetric structure. The conduction band potential profiles under bias for the symmetric and asymmetric structures are also shown, demonstrating the misalignment of the QW states for the symmetric structure, (figure 1(d)), and alignment of the $n = 1$ QW states for the asymmetric structure, (figure 1(f)).

3. Results and discussion

Current–voltage ($I(V)$) characteristics for the symmetric QW structure, at very low forward bias, within a temperature range 3–293 K are shown in figure 2. The feature of interest for this paper is the peak labelled X, which appears as the sample temperature is raised. The peak increases in magnitude with temperature and shows a small NDR region which is discernible even at 293 K. The shift in peak position to higher voltages with increasing sample temperature is attributed to an increase in series resistance. If we consider a totally symmetrical structure at zero bias the electron probability density of the quasi-confined states is equally distributed between both QWs and therefore we take the QW states to be aligned, as shown in figure 1(c). Electrons incident on the emitter barrier whose energy is equal to the aligned states of the two QWs have a high theoretical probability of transmission ($T(E)$). (The transmission probability is not necessarily equal to unity for a symmetric well TBRTS, but has been shown to be dependent on the barrier widths in the TBRTS design [22]). Conventionally, to instigate tunnelling a voltage is applied to the device. Applying an electric field however destroys the alignment of the QW states in this symmetric QW structure, localizing each state to a specific QW

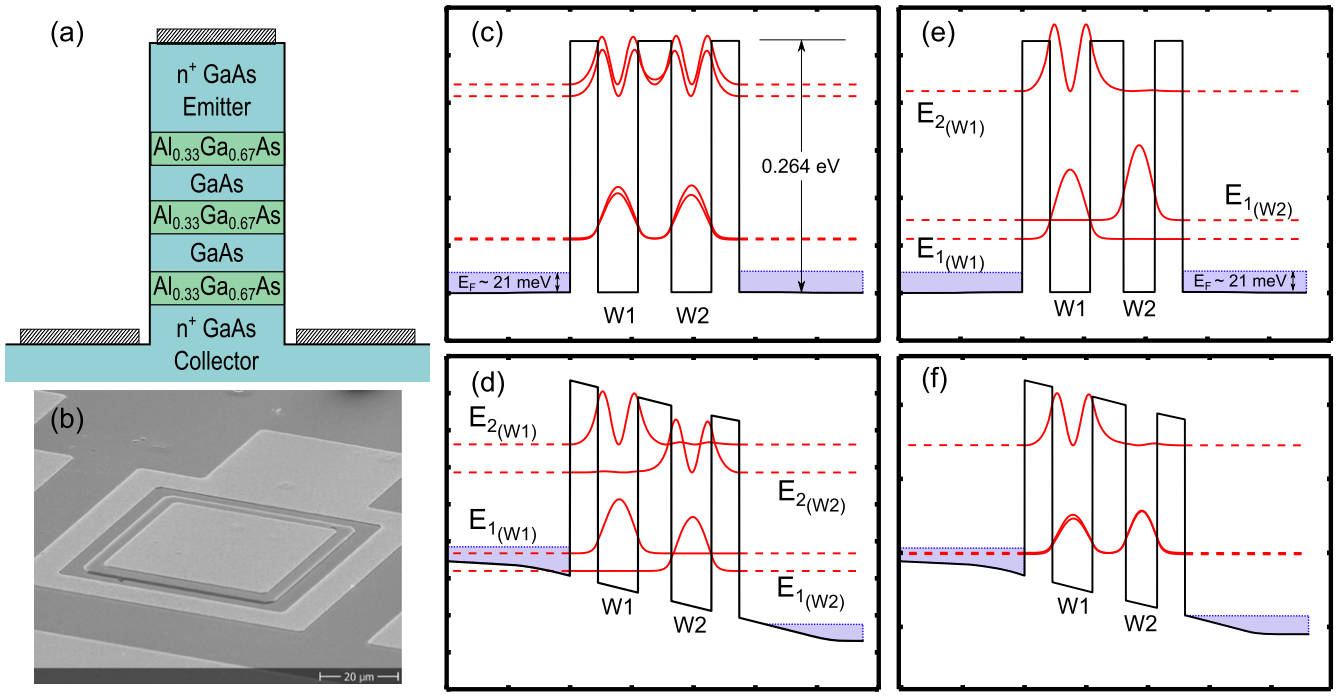

Figure 1. (a) A cross section schematic of a fabricated TBRTS device showing the layer structure; (b) SEM image of a 50 × 50 μm mesa fabricated TBRTS device; (c) conduction band potential profile for a symmetric structure at zero bias, where QW (*W*1) is the same width as QW (*W*2). The Fermi energy in the emitter and collector regions at approximately 21 meV above the conduction band edge are also shown with the calculated electron probability density showing alignment of the $n = 1$ and $n = 2$ QW states; (d) the symmetric structure under bias. The electron probability density shows the $n = 1$ states are misaligned and localized to a specific QW ($E_{1_{(W1)}}$ for W1 and $E_{1_{(W2)}}$ for *W*2); (e) an asymmetric structure at zero bias, the calculated electron probability density shows the $n = 1$ states are misaligned and localized to a specific QW ($E_{1_{(W1)}}$ for *W*1 and $E_{1_{(W2)}}$ for *W*2). Only one $n = 2$ QW state ($E_{2_{(W1)}}$) which is localized to *W*1 is allowed due to the decreased width of *W*2; (f) an asymmetric structure under bias, the electron probability density shows alignment of the $n = 1$ QW states.

($E_{1_{(W1)}}$, $E_{1_{(W2)}}$, $E_{2_{(W1)}}$ and $E_{2_{(W2)}}$) as shown in figure 1(d), thus reducing the overall transmission probability. The structure only has a high transmission essentially at zero bias and therefore is extremely hard to exploit electrically since any applied voltage will invariably alter the symmetry of the active region. A possible solution to this problem is to use a three terminal device where the injection energy is controlled by an emitter base voltage across a DBRTS, while the base collector voltage across the TBRTS active region is maintained at zero bias [23]. However this would be difficult to implement since the base region must be of the order of the ballistic length of the carriers to successfully maintain the precise injection energy.

If however the sample temperature is raised, a significant number of electrons in the emitter region are thermally promoted to energies equal to the $n = 1$ subband energy of the aligned QWs at zero bias. On application of a small forward bias these electrons can tunnel through the TBRTS, which will remain highly transparent provided the bias is small enough to cause negligible perturbation to the symmetry of the QW regions. A reasonable estimate of this can be made by calculating the broadening of the state from calculating a simple transmission coefficient using a transfer matrix method, as a function of energy. The full-width half maximum of the $n = 1$ subband peaks were taken as the broadening of the states and a linear voltage drop model was then applied to calculate the amount of bias required to misalign the $n = 1$ states, which in this case gives approximately 6.6 mV. Due to the very high transparency of symmetrical devices this causes a significant rise in the device current at extremely low bias. As the bias is increased further the $n = 1$ states become more localized to the collector and emitter QWs, with the collector QW ($E_{1_{(W2)}}$) state dropping below that of the emitter QW state ($E_{1_{(W1)}}$), thus the two $n = 1$ QW states go out of alignment and the high transmission probability is lost. We attribute the peak labelled X in figure 2 to such a process, where thermal activated electrons tunnel through the aligned $n = 1$ states of the QWs. Forcing the QW states out of alignment results in the NDR region observed in the temperature range 121–293 K.

It is important to stress that this is very different to the behaviour of conventional DBRTS where the single level remains transparent to an increasing number of electrons as the bias is increased and the QW state is moved lower in energy relative to the electron distribution in the emitter. This phenomena therefore is purely associated with multiple ($\geqslant 3$) barrier structures where the application of an electric field alters the transmission properties of the tunnelling region, and not just the effective incident electron injection energies.

This description of the thermally activated resonant tunnelling peak assumes that the QW confined states are aligned at zero bias. In a symmetric QW device alignment occurs at zero bias, however in an asymmetric structure where the QWs have different widths this is not the case,

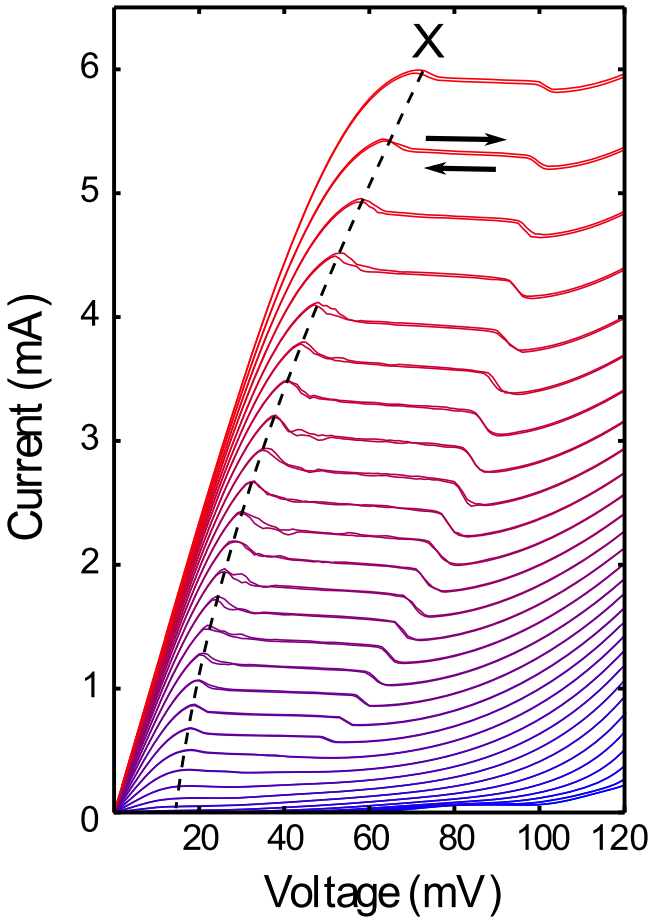

Figure 2. Low bias, current–voltage ($I(V)$) characteristics between 3 K (low current) and 293 K (high current) at 10 K intervals, for the nominally symmetric 65 Å QW GaAs/AlGaAs TBRTS. The $I(V)$ characteristics are not adjusted to take into account any series resistance and only shown at 10 K intervals for clarity. A small amount of current hysterisis can be seen between the forward and reverse going sweeps (indicated by arrows). A dashed (black) line guides the eye to the evolution of peak X with temperature.

(figure 1(e)). Thermally activated resonances are observed in both bias directions for a perfectly symmetric structure, but if the collector QW is narrower than the emitter QW the confined states are only aligned by an appropriate forward bias, (figure 1(f)). In reverse bias the $n = 1$ states of the emitter and collector QWs are never energetically aligned.

Due to the high currents passing through the devices, pulsed voltage $I(V)$ characteristics were measured for the most asymmetric structure, figure 3(a). The pulsed $I(V)$ characteristics show negligible deviation from the continuous voltage sweep measurements and as such it is assumed there is negligible device self heating. To enable a more quantitative analysis of this tunnelling feature an exponential fit of the form $y = Ax^2 \exp(Bx) - Ax^2$ has been made to the background leakage current and subtracted from the series resistance adjusted data, shown for the nominally symmetric structure at 3 K in figure 3(b).

Figure 4 shows forward $I(V)$ characteristics at 3 K (figure 4(a)) and 121 K (figure 4(b)) for a series of increasingly asymmetric devices where the second QW width is reduced by nominally a monolayer for each sample. The low bias resonant current peak at point (i) is not seen at 3 K for the more symmetric devices (red dashed line), and only becomes visible at higher temperatures (increases in magnitude as the sample temperature is raised), figure 4(b), or with increased asymmetry. The NDR region of this peak becomes more pronounced as the asymmetry of the structure is increased and results in instabilities in the NDR region. This peak is attributed to the alignment of the $n = 1$ confined QW states ($E_{1_{(W1)}}$ and $E_{1_{(W2)}}$) in each case as previously described. As can be seen from figure 4(b) the peak occurs at increasingly higher values of bias as the width of the second QW is decreased. This reflects the increase in bias required to align the QW states as the ground state confinement energy in the collector QW is increased. The peak also becomes discernible at progressively lower temperatures as the collector well width is decreased, due to the alignment of the QW states occurring closer in energy to the Fermi level in the emitter region, figure 4(a) (asymmetric structures).

Non-thermally activated current peaks are also seen in figures 4(a) and (b), a small peak at (ii) is discernible at low temperatures which is associated with the alignment of the collector $n = 1$ QW state ($E_{1_{(W2)}}$) and the populated 3D states in the emitter region ($E_{M_{3D}}$). This feature is small in magnitude and so is concealed by thermal leakage current at higher temperatures. Alignment of the emitter $n = 1$ QW state ($E_{1_{(W1)}}$) with the populated 3D states in the emitter region ($E_{M_{3D}}$) also occurs and is labelled (iii) in figures 4(a) and (b). This peak exhibits a region of NDR and instability and remains on resonance over a larger voltage range than would necessarily be expected and can be explained by charge accumulation in the emitter QW [19]. The feature remains relatively stationary in voltage with increasing asymmetry of the structure until it begins to merge with features (i) and (ii) and it is at this point (iv), where the alignment of the $n = 1$ emitter QW ($E_{1_{(W1)}}$), collector QW ($E_{1_{(W2)}}$) and populated 3D emitter ($E_{M_{3D}}$) states occur coincidentally. This can be seen in the case of the highly asymmetric QW structure at 3 K, where the resonant peak is still observed. Here the alignment of the QW energy levels is virtually coincident with the Fermi level in the emitter and so it is therefore probably misleading to describe this peak as thermally activated. The proximity of the Fermi level in the emitter with respect to the aligned states therefore accounts for the significant increase in current through this device at 3 K. The thermally activated tunnelling peak can be used as a sensitive characterization tool to monitor the QW state alignment in such structures, and therefore device symmetry. The feature labelled (v) is associated with the alignment of the $n = 2$ QW state in the collector ($E_{2_{W2}}$) with the populated 3D states in the emitter region ($E_{M_{3D}}$). With increasing structure asymmetry the bias required to produce this alignment increases due to the confinement energy of the collector QW state increasing. For the two most asymmetric structures this feature is no longer observed as the collector QW is too narrow for an $n = 2$ confined state to exist within the QW.

Experimentally extracted Arrhenius plots of the magnitude of the thermally activated peak current after background

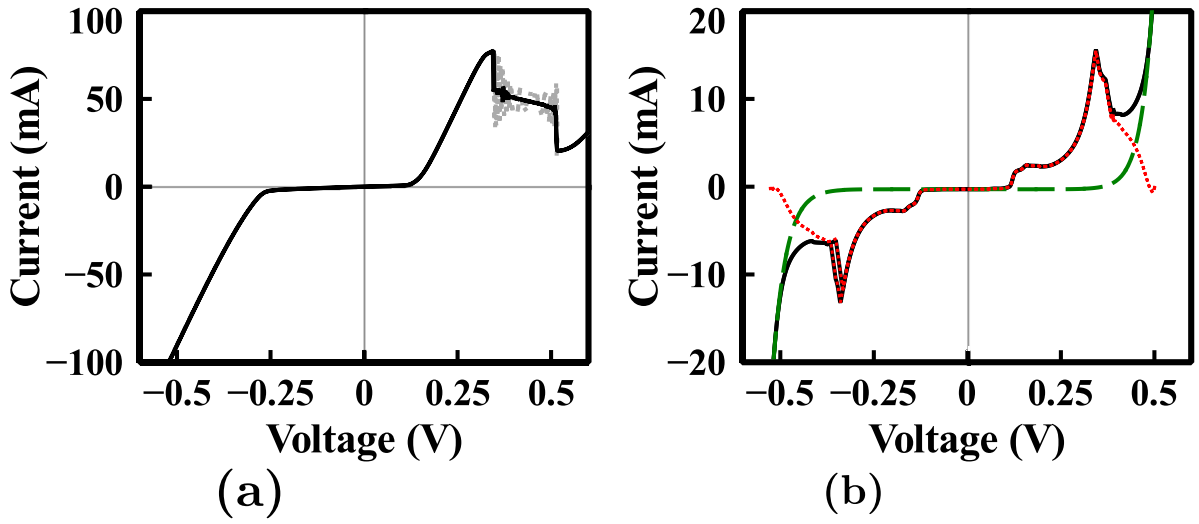

Figure 3. (a) $I(V)$ characteristic for the most asymmetric structure (solid black line), with a pulsed voltage $I(V)$ characteristic overlayed (grey dotted line). The 1% duty cycle pulses of 0.5 ms width demonstrates no significant device heating in the CW (continuous wave) measurement over the entire voltage range; (b) $I(V)$ characteristics for the nominally symmetric structure between ±0.6 V at 3 K. A series resistance adjusted $I(V)$ (solid black line), background leakage current adjusted characteristic (red dotted line) and the background exponential fit of the form $y = Ax^2 \exp(Bx) - Ax^2$ made to the background leakage current (green dashed line) are shown.

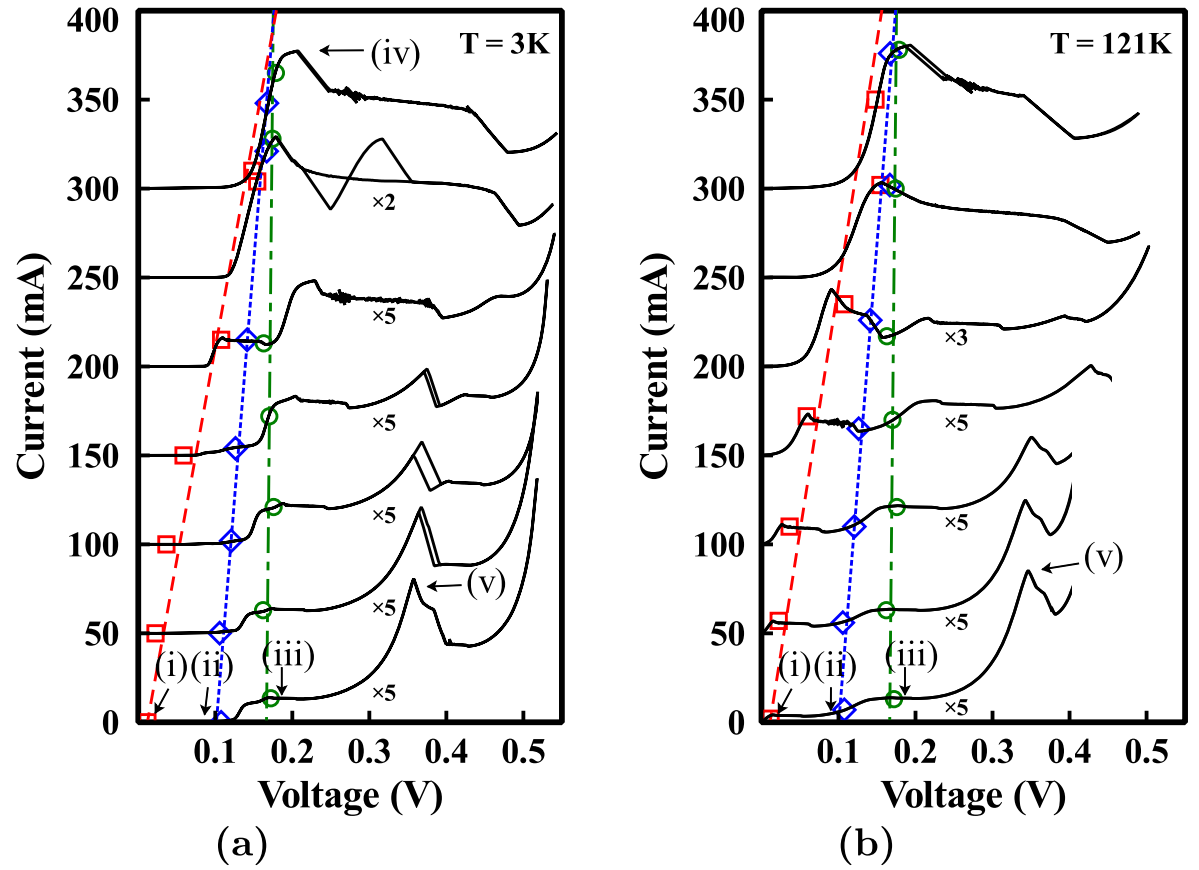

Figure 4. (a) Series resistance corrected current–voltage ($I(V)$) characteristics for a range of increasingly asymmetric QW TBRTS at 3 K. The $I(V)$ characteristics for different structures are offset by 50 mA for clarity. The predicted resonance voltages from a simple linear voltage drop model are indicated by red squares, blue diamonds and green circles for alignment conditions (i), (ii) and (iii) respectively; (b) 121 K $I(V)$) characteristics for a range of increasingly asymmetric QW TBRTS. The thermally activated resonance (red dashed line) is clearly visible in all structures at this temperature.

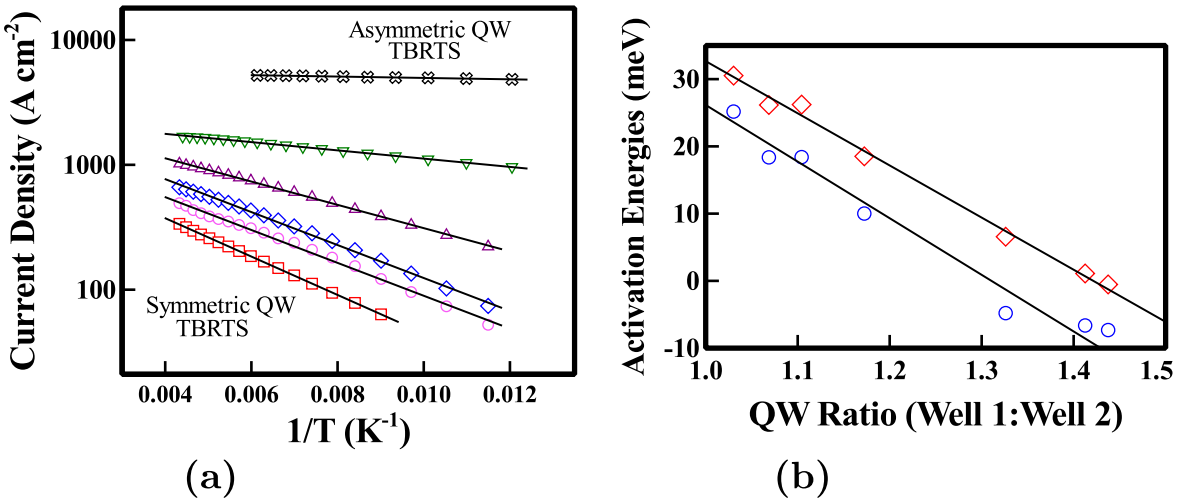

Figure 5. (a) Experimentally determined Arrhenius plots of the thermally activated peak current density attributed to the $n = 1$ QW state alignment. The nominally symmetric to highly asymmetric triple barrier resonant structures are shown with every fourth data point plotted between 73 K and 231 K; (b) the experimentally determined (red diamonds), and theoretically calculated (blue circles) activation energies against the ratio of quantum well (QW) widths ($W1$:$W2$). The QW widths are taken from photoluminescence excitation (PLE) measurements.

leakage and series resistance adjustment for each sample are plotted in figure 5(a). The gradient of the resulting straight lines, which involves a change in current of close to three decades, is used to extract an activation energy. This activation energy decreases as the second well width is decreased, due to alignment occurring at an increasingly larger bias, and at an energy closer to the Fermi level in the emitter region.

Theoretical activation energies were calculated by modelling the number of charge carriers available for tunnelling at energies equal to those of the aligned $n = 1$ QW states. The number of carriers is proportional to the tunnelling current through the resonantly aligned states and as such activation energies determined in this way should give good agreement to experimentally determined values. The modelling for the devices was done in two parts. Firstly a linear electric field was applied across the undoped spacers and active region of the structure. This is a good first approximation as the applied voltage is predominantly dropped between the n+ doped buffer layer and the δ-doped layer at low bias. For each potential profile Schrödinger's equation was solved within only the active region of the device and infinite potential barriers were assumed outside of this region. The bound state energy and wave function for each state was found and the bias increased until alignment of the $n = 1$ QW states occurred. Secondly, at the bias required for alignment the number of charge carriers available for tunnelling at energies equal to those of the aligned bound states was found by integrating the product of the 3D density of states and the Fermi function between the energies of the symmetric and anti-symmetric $n = 1$ bound states in the active region. This calculation was repeated for temperatures between 73 K and 231 K and fitting of the resultant carrier density against T^{-1} using the full Fermi–Dirac distribution allows for the extraction of a theoretical activation energy. Figure 5(b) shows the theoretical activation energies determined in this way alongside the experimentally determined values. The theoretical model utilizes experimentally determined well width data derived from photoluminescence excitation (PLE) measurements that monitored the intensity of the bulk GaAs luminescence at zero bias as a function of excitation energy. For details of these measurements and the well width extraction see reference [24]. The agreement between the experimental activation energies and those obtained theoretically is good and experimental observation is supported by the general trends observed in the theoretically derived data.

4. Conclusion

In conclusion, we have observed a current peak in the $I(V)$ characteristic of TBRTS with both symmetric and asymmetric QWs, which increases in magnitude with sample temperature. The peak is attributed to thermally activated electrons tunnelling through the confined ground states ($n = 1$) of the two QWs in the TBRTS which have been energetically aligned by the application of a forward bias. Activation energies for this tunnelling process have been experimentally determined and compared to theoretical prediction. They have been used to demonstrate QW ground state energy alignment where this alignment occurs at a greater energy than the Fermi energy in the emitter. This resonance effect becomes stronger with increasing temperature, unlike the resonance observed in conventional DBRTS. This may prove useful for practical application of negative resistance tunnelling devices at high temperature.

Acknowledgments

The authors would like to acknowledge funding from the UK Engineering and Physical Sciences Research Council. Data supporting this research is openly available from the Cardiff

University Research Portal at http://dx.doi.org/10.17035/d.2015.100109.

References

[1] Asada M, Oguma Y and Sashinaka N 2000 *Appl. Phys. Lett.* **77** 618–20
[2] Ishigaki K, Shiraishi M, Suzuki S, Asada M, Nishiyama N and Arai S 2012 *Electron. Lett.* **48** 582–3
[3] Suzuki S, Shiraishi M, Shibayama H and Asada M 2013 *IEEE J. Sel. Top. Quantum Electron.* **19** 8500108
[4] Kanaya H, Shibayama H, Suzuki S and Asada M 2012 Fundamental oscillation up to 1.31 thz in thin-well resonant tunneling diodes *2012 Int. Conf. Indium Phosphide and Related Materials* (*IPRM*) pp 106–9
[5] Feiginov M, Kanaya H, Suzuki S and Asada M 2014 *Appl. Phys. Lett.* **104** 243509
[6] Mizuta H, Tanoue T and Takahashi S 1988 *IEEE Trans. Electron Devices* **ED-35** 1951–6
[7] Tanoue T, Mizuta H and Takahashi S 1988 *Electron Device Lett.* **9** 365–7
[8] Waho T, Chen K and Yamamoto M 1996 *IEEE Electron Device Lett.* **17** 223–5
[9] Faist J, Capasso F, Hutchinson A, Pfeiffer L and West K 1993 *Phys. Rev. Lett.* **71** 3573–6
[10] Strutz T and Shiraki Y 1996 *Semicond. Sci. Technol.* **11** 103–6
[11] Roskos H, Nuss M, Shah J, Leo K, Miller D, Fox A, Schmitt-Rink S and Köhler K 1992 *Phys. Rev. Lett.* **68** 2216–9
[12] Truscott W S 1993 *Phys. Rev. Lett.* **70** 1900–3
[13] Buckle P, Dawson P, Lynch M, Kuo C Y, Missous M and Truscott W 2000 *IEEE Trans. Microw. Theory Tech.* **48** 632–8
[14] Brown E R, Soderstrom J R, Parker C D, Mahoney L J, Molvar K M and McGill T C 1991 *Appl. Phys. Lett.* **58** 2291–3
[15] Soderstrom J R, Yao J Y and Andersson T G 1991 *Appl. Phys. Lett.* **58** 708–10
[16] Nakagawa T, Imamoto H, Kojima T and Ohta K 1986 *Appl. Phys. Lett.* **49** 73–75
[17] Nakagawa T, Fujita T, Matsumoto Y, Kojima T and Ohta K 1987 *Japan. J. Appl. Phys.* **26** L980
[18] Kim G, Koh K M and Kim C H 2001 *Superlattices Microstruct.* **29** 51 – 55
[19] Buckle P, Dawson P, Kuo C, Roberts A, Truscott W, Lynch M and Missous M 1998 *J. Appl. Phys.* **83** 882–7
[20] Nakagawa T, Fujita T, Matsumoto Y, Kojima T and Ohta K 1987 *Appl. Phys. Lett.* **51** 445–7
[21] Ozaki S, Feng J M, Park J H, Osako S i, Kubo H, Morifuji M, Mori N and Hamaguchi C 1998 *J. Appl. Phys.* **83** 962–5
[22] Leo J and Toombs G 1991 *Phys. Rev.* B **43** 9944–6
[23] Capasso F, Sen S, Beltram F, Lunardi L M, Vengurlekar A S, Smith P R, Shah N J, Malik R J and Cho A Y 1989 *IEEE Trans. Electron Devices* **36** 2065–82
[24] Buckle P, Dawson P, Missous M and Truscott W 1997 *J. Cryst. Growth* **175–176** 1299–302